Investigation of soil desiccation cracking using an environmental chamber

Yu-Jun Cui,* Chao-Sheng Tang,** Anh Minh Tang,* An Ninh Ta*

Summary

Soil desiccation cracking due to loss of water is a common natural phenomenon, and can significantly affect the soil performance in various geotechnical, geological and environmental engineering applications. In this investigation, a large-scale environmental chamber (1 m × 0.8 m × 1.5 m) was developed for carrying out physical model desiccation tests. This chamber was instrumented by various sensors allowing the soil volumetric water content and suction to be monitored at various depths. The air temperature and relative humidity at the inlet, in the chamber and at the outlet can also be monitored. The development of cracks on soil surface was monitored by a camera which was fixed above the chamber. The soil column was subjected to a 30-day drying under controlled air conditions. The results show that the average actual evaporation rate of soil column is constant at the initial stage of drying and then tends to decrease with decreasing water content. Cracks initiate at very high water content (about 60 %) when the soil is still saturated and the corresponding evaporation rate is constant. By image processing, the evolution of geometrical and morphological parameters of the crack networks was quantitatively analysed. It is found that the crack parameters reach stabilization at different water contents during drying. The number of clods, nodes and crack segments reach stabilization earlier than the average crack length and crack density. The evolution characteristics of surface crack ratio and average crack width are highly consistent, and in addition, they are the last to reach stabilization. The results indicate that the developed environmental chamber constitutes an effective tool for studying the desiccation cracking behaviour of soil in large scale, and provides useful data for the investigation of soil-atmosphere interactions.

Keywords: environmental chamber; desiccation cracking; soil water evaporation; image processing; suction; volumetric water content

Introduction

Soil-vegetation-atmosphere interaction has become a main concern in geotechnical engineering, especially for slope stability analysis [Ridley, 2012, Pirone *et al.* 2012 and Askarinejad *et al.* 2012]. Evaporation of water usually results in soil volumetric shrinkage. When the shrinkage is constrained and the induced tensile stress reaches the soil tensile strength, desiccation cracks occur. This phenomenon can involve many earth structures such as dams, hydraulic barriers, slopes, runway sub-grades, river banks, highway and railway embankments. Previous investigations evidenced that the presence of desiccation cracks significantly modifies both the mechanical and hydraulic properties of soils. For instance, cracks affect soil compressibility, consolidation rate and strength [Morris *et al.* 1992]. The geotechnical and geological aspects of construction are affected directly or indirectly by the presence of soil cracks. A cracked soil has much higher hydraulic conductivity than an intact one, since cracks constitute preferential pathways for water flow [Albrecht and Benson 2001]. In geo-environmental engineering applications, high-plasticity clayey soils with low hydraulic conductivity are widely used in constructing landfill liners, covers and slurry walls for containment of solid or liquid wastes. However, these clayey soils are susceptible to desiccation cracking during drought. The performance of containment barriers is therefore significantly affected by dessication and subsequent cracking of soils. Cracking leads to a degradation of the containment function of the liner, which can result in an increase in infiltration of surface water into the containment system or migration of the contained liquids into the surrounding soils and groundwater, and can also lead to a decrease in integrity and structural stability of the containment system [Miller *et al.,* 1998]. Cracks may also compromise the water retention capacity of dams, leading to failures as reported by Sherard [1973]. In other circumstances of exposed terrain, cracking often implies that groundwater recharge can take place more quickly than drawdown, a situation that can lead to instability of natural slopes and vertical cuttings [Baker, 1981], and to a decrease of the bearing capacity of foundations [Silvestri *et al.*,1992].

In the past decades, a large number of experimental tests have been conducted aiming at understanding the initiation and propagation mechanisms of desiccation cracks [Corte and Higashi, 1960; Miller *et al.,* 1998 ; Rodríguez *et al.,* 2007; Péron *et al.,* 2009; Tang *et al.,* 2011a], quantifying and characterizing the

* Ecole des Ponts - ParisTech, UR Navier-CERMES, Cité Descartes, Champs-sur-Marne, Marne-la-Vallée, France
* School of Earth Sciences and Engineering, Nanjing University, Nanjing, China

crack patterns [YESILLER *et al.,* 2000; LAKSHMIKANTHA *et al.,* 2009; TANG *et al.,* 2011b], investigating the influencing factors of desiccation cracking [ALBRECHT and BENSON, 2001; NAHLAWI and KODIKARA, 2006; TANG *et al.* 2008; TANG *et al.,* 2010; LAKSHMIKANTHA *et al.,* 2012], examing the role of additives in improving soil cracking resistance [MILLER and RIFAI, 2004; HARIANTO *et al.,* 2008; TANG *et al.,* 2012], etc. However, most studies on soil desiccation cracking behaviour have only been carried out on small size and thin soil specimens. Despite the convenience and low cost, there is increasing concern about the representativity of the results obtained on this kind of specimens.

In this study, a large scale physical model desiccation test was conducted using a specially developed environmental chamber. During drying, the crack initiation and propagation processes were monitored as well as the profiles of soil water content and suction. The geometrical and morphological characteristics of the crack patterns were quantitatively analysed using image processing technique.

Material and method

Material

The Romainville clay taken from the eastern region of Paris was used for this study. Its basic geotechnical properties were investigated by AUDIGUIER *et al.* [2007] and LARIBI *et al.* [2008], and are shown in table I. From the relatively high values of Atterberg's limits (liquid limit of 75 %; plastic limit of 40% and plasticity index of 35), large fraction (84 %) of clay-size particles (< 2 μm) and large specific surface (98 m^2/g), it can be deduced that this soil is of expansive nature.

Tab. I – Geotechnical properties of Romainville clay [AUDIGUIER *et al.,* 2007; LARIBI *et al.,* 2008].
Tab. I – Caratteristiche geotecniche dell'argilla di Romainville.

Property	Values
Specific gravity	2.67
Liquid limit	75%
Plastic limit	40%
Plasticity index	35%
USUC classification	CH
Clay (<2μm)	84%
Carbonate content	15-20%
Specific surface area	98 m^2/g

The soil taken from the site was air dried in the laboratory to reach a gravimetric water content of 5.7 % and then crushed and passed through a 2 mm sieve.

Eexperimental set-up

A special environmental chamber (inner dimensions: L × W × H: 1000 × 800 × 1550 mm) was developed for performing the large scale physical mold desiccation test. A schematic drawing and a picture are presented in figure 1. The chamber consists of six acrylic plates (20 mm thick) joined together by epoxy glue. The bottom of chamber is fixed on a polyvinyl chloride plate (30 mm thick). The system is strengthened by four vertical metallic stiffeners on the four corners and confined by several lateral metallic stiffeners in order to provide good resistance against the lateral stress exerted by the soil. The joints between the plates are finally sealed by silicon glue to prevent any leakage.

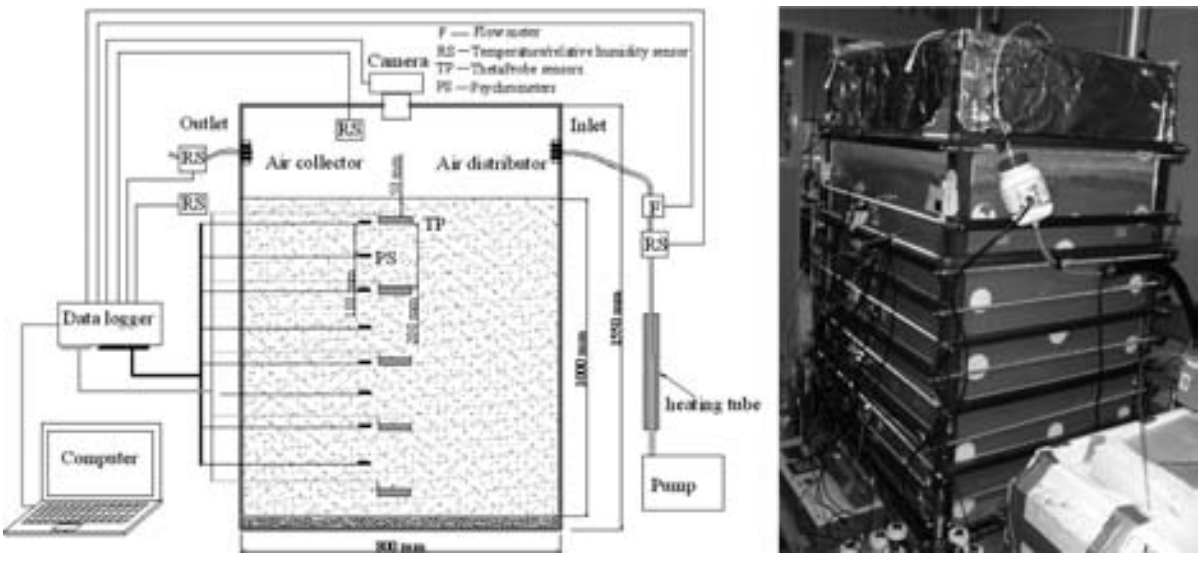

a) b)

Fig. 1 – Schematic drawing a) and a photo of the environmental chamber b).
Fig. 1 – Schema a) e fotografia b) della camera ambientale.

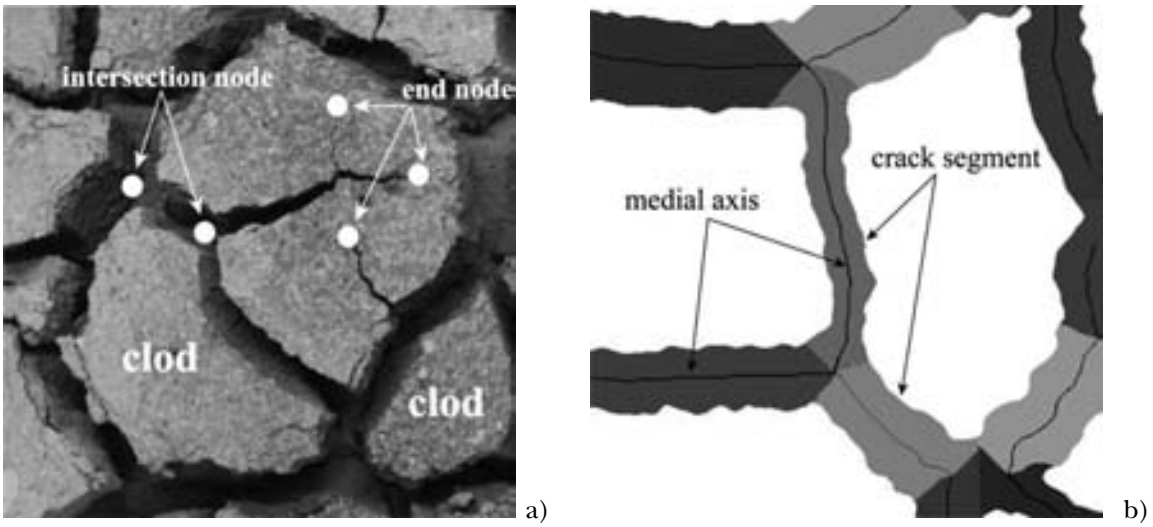

Fig. 2 – Crack pattern: a) typical original crack pattern obtained during drying; b) typical crack pattern after image processing.
Fig. 2 – Stato di fratturazione: a) stato di fratturazione tipico originale, ottenuto con l'essiccamento; b) stato di fratturazione tipico dopo l'elaborazione dell'immagine.

The soil column in the chamber was prepared by compaction in layers of 50 mm each to a dry density of 1.35 Mg/m^3, similar to the in-situ dry density [CUI *et al.,* 2006]. The final height of the soil column is 1000 mm. Several sensors were installed in the soil column through two opposite walls of the chamber: 5 ThetaProbe sensors (TP) for the measurement of volumetric water content were buried every 200 mm; the measurement range of TP is 0-100 % and the accuracy is ± 0.1 %; 8 psychrometers (PS) for the measurement of total suction were installed every 100 mm; the measurement range of PS is 0.05-8 MPa and the accuracy is ± 0.03 MPa. All the sensors buried in the soil were installed during compaction.

In order to control the evaporation rate of soil column, a ventilation system was installed in the upper part of the chamber. Flow rate controlled air was injected into the chamber from the inlet. The air flow rate was measured using a flowmeter F (±2 % accuracy over a working range of 500 L/min). Thanks to a heating tube, air was heated and the heated air was monitored by a RS sensor giving the actual temperature and relative humidity before being diffused into the chamber through the 8 holes of an air distributor. The RS sensor has a range from -30 to 150 °C to an accuracy of ± 0.4 °C for temperature, and a range from 0 to 100 % to an accuracy of ± 2.5 % for relative humidity. At the outlet of the chamber, the air was gathered by an air collector where temperature and relative humidity were again measured. In order to monitor cracks at the soil surface during drying, a high definition camera was fixed over the chamber. Furthermore, RS sensors were also installed inside the chamber in the zone occupied by air and outside the chamber (placed about 0.5 m away from the top cover of the chamber).

Test procedures

After the soil column was compacted in the chamber, the system was sealed. In order to verify the performance of the system, an initial short-term wetting (3 days) and drying (25 days) cycle was applied to the soil column. After that, the soil column was rewetted from the surface for a long period of 265 days. The recorded data showed good performance of all sensors installed in the soil. The detailed results during the subsequent long drying period can be found in CUI *et al.* [2013]. Note that at the end of the rewetting stage, most of the soil column was saturated at a volumetric water content of nearly 50 %, the volumetric water content of the first 50 mm from the surface being much higher (77 % at 50 mm depth) because of the large soil swelling in this zone [TANG *et al.,* 2009].

In this study, the dried soil column has been immerged under water for a long period of 256 days to saturate the soil column and then subjected to a second drying process by injecting heated air at a flow rate of 1.67×10^{-3} m^3/s (100 L/min). A thin water layer of about 20 mm was present on the soil surface at the beginning of drying. The drying test took 30 days. The temperature and relative humidity measured at the inlet and outlet of the chamber were used to calculate the actual evaporation rate following the method reported by MOHAMED *et al.* [2000].

Quantification of crack pattern

Once desiccation cracks appeared on the soil surface, the camera took photos every 90 min. By image processing, the recorded crack patterns were quantitatively characterized. The following parame-

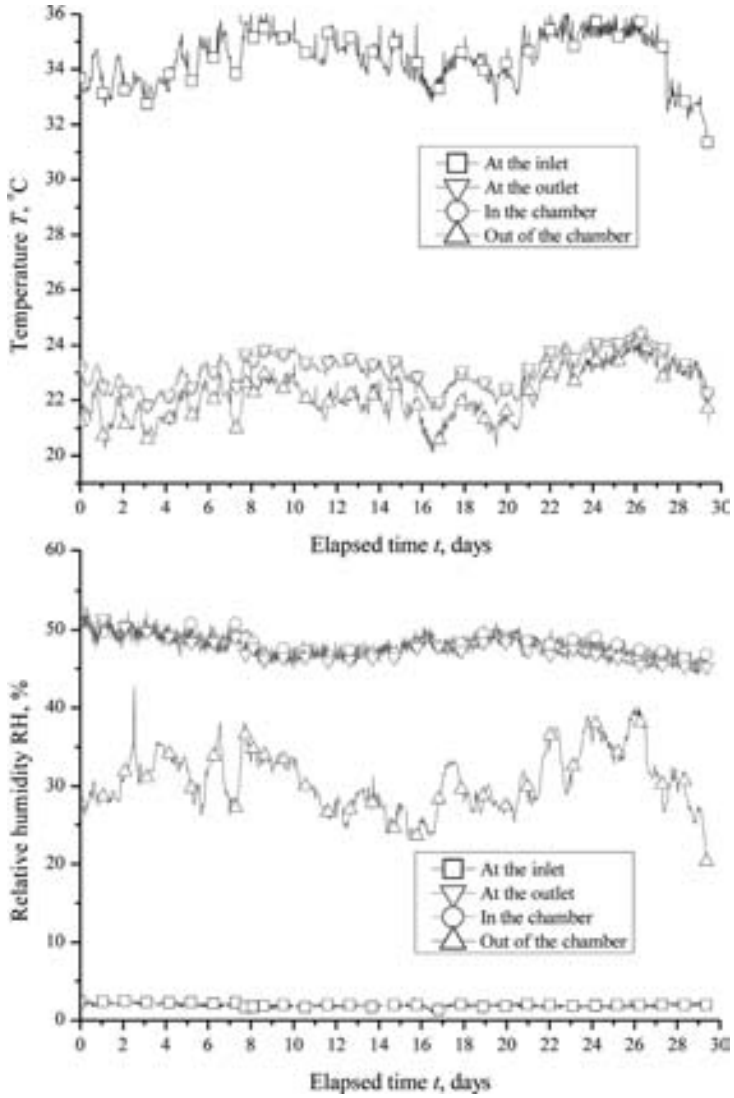

a)

b)

Fig. 3 – Variations of air temperature a) and air relative humidity b).
Fig. 3 – Variazione nel tempo della temperatura dell'aria a) e dell'umidità relativa dell'aria b).

ters were determined allowing the discription of the geometrical and morphyologic characteristics of the crack networks:

1) Surface crack ratio R_{sc}, which is the ratio of the crack area to the total surface area of soil column.
2) Number of clods N_c and average area of clods A_{av}. The clod is defined as the independent closed area which is bounded by cracks (Fig. 2a).
3) Number of nodes N_n and number of crack segments N_{seg}. Two types of nodes are considered: intersection nodes between crack segments and end nodes of single crack without intersecting each other (Fig. 2a).
4) Average length of cracks L_{av}, and average width of cracks W_{av}. The crack length is determined by calculating the trace length of the medial axis of crack segment, as illustrated in figure 2b. The average width of cracks W_{av} is calculated by dividing the total crack area by the total crack length.
5) Crack density D_c, which is defined as the crack length per unit soil surface, namely the ratio of total crack length to the total soil surface.

Note that only the central part (920 mm ×705 mm) of the crack pattern was used for image processing so as to minimize the boundary effect. Detailed information about the image processing procedures and crack parameters identification can be found in TANG *et al.* [2008].

Results and discussion

Actual evaporation rate

The evolutions of the air temperature and the air relative humidity at the inlet, at the outlet, in the chamber, out of the chamber are shown in figure 3. It

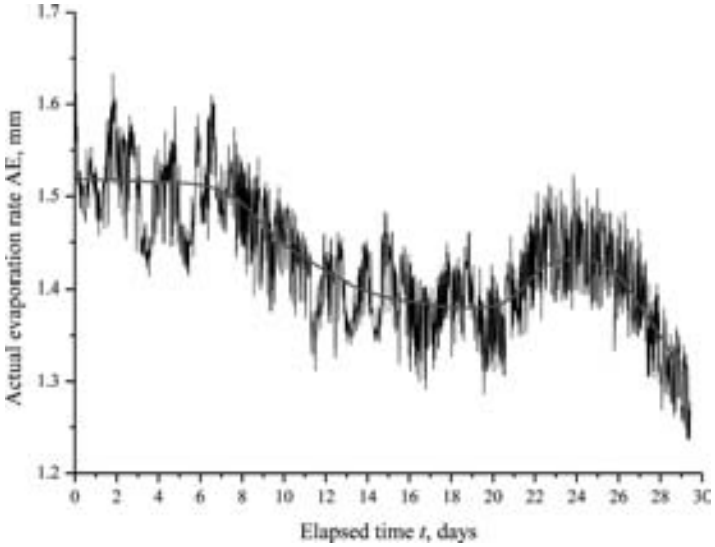

Fig. 4 – Variation of actual evaporation rate and the average value.
Fig. 4 – Variazione nel tempo del tasso di evaporazione e andamento medio.

can be seen from figure 3a that the variation trend of temperature at the inlet, at the outlet and in the chamber is similar to that of the ambient temperature, indicating that the temperature of the chamber system is generally conditioned by the ambient temperature. The mean values of temperature (about 23 °C) in the chamber and at the outlet are very close, slightly higher than the ambient temperature (about 22 °C) but much lower than that at the inlet (about 34 °C). This is due to the fact that part of the thermal energy from the inlet was consumed for soil water evaporition.

As far as the relative humidity is concerned (Fig. 3b), the value at the inlet is tiny and close to zero due to heating. The ambient relative humidity presents significant variations (25-50 %) and seems to have no influence on the values at the inlet, at the outlet and in the chamber. The values in the chamber and at the outlet are close and much higher than the value at the inlet, indicating that evaporation occured in the chamber. In addition, they both present a regular decrease from 53 to 45 % over time. It can be deduced that the injected air flow in the chamber was not laminar but probably turbulent. The measured RH values in the chamber reflect the average level. This explains why the measured RH values in the chamber and at the outlet are quite similar.

Based on the temperature and relative humidity measured at the inlet and outlet during drying, the actual evaporation rate (AE) is calculated, as follows:

First, the saturated vapor pressure P_v^s is calculated [BRUTSAERT, 1988]:

$$P_v^s = 101.325\exp(13.3185t_R - 1.9760t_R^2 - 0.6445t_R^3 - 0.1299t_R^4) \quad (1)$$

where $t_R = 1 - (373.15 / T)$ in which T is the temperature in K.

Second, the vapor pressure P_v is calculated:

$$P_v = 100hP_v^s \quad (2)$$

where h is the air relative humidity.

Third, the density of water vapor ρ_v is deduced:

$$\rho_v = \frac{0.622P_v}{RT_a} \quad (3)$$

where the value of 0.622 is the ratio of the molecular weights between water and dry air, R is gas constant (R = 8.3143 J/mol/K) and T_a is the air temperature.

Finally, the difference of water vapor density of air at the inlet ρ_{v_inlet} and at the outlet ρ_{v_outlet} is used to calculate the evaporation rate AE:

$$AE = q(\rho_{v\_outlet} - \rho_{v\_inlet}) \quad (4)$$

where q is the air flow rate.

The results obtained are presented in figure 4. It can be observed that, during the initial drying stage (from t =0 to t = 6 days), the average AE generally varies around 1.52 mm/day. It is probably due to the high water content or degree of saturation of soil in this stage. As mentioned above, a thin water layer was kept on the soil surface before drying. The water supply for evaporation is therefore sufficient. Previous studies demonstrated that, under constant drying conditions (i.e. constant ambient temperature, relative humidity, etc.), the actual rate of evaporation from saturated soil surface is theoretically constant and equal to the rate of evaporation from an open or free water surface. Once the soil becomes unsaturated, the evaporation rate starts to decrease gradually [WILSON *et al.*, 1997]. Figure 4 shows that upon further

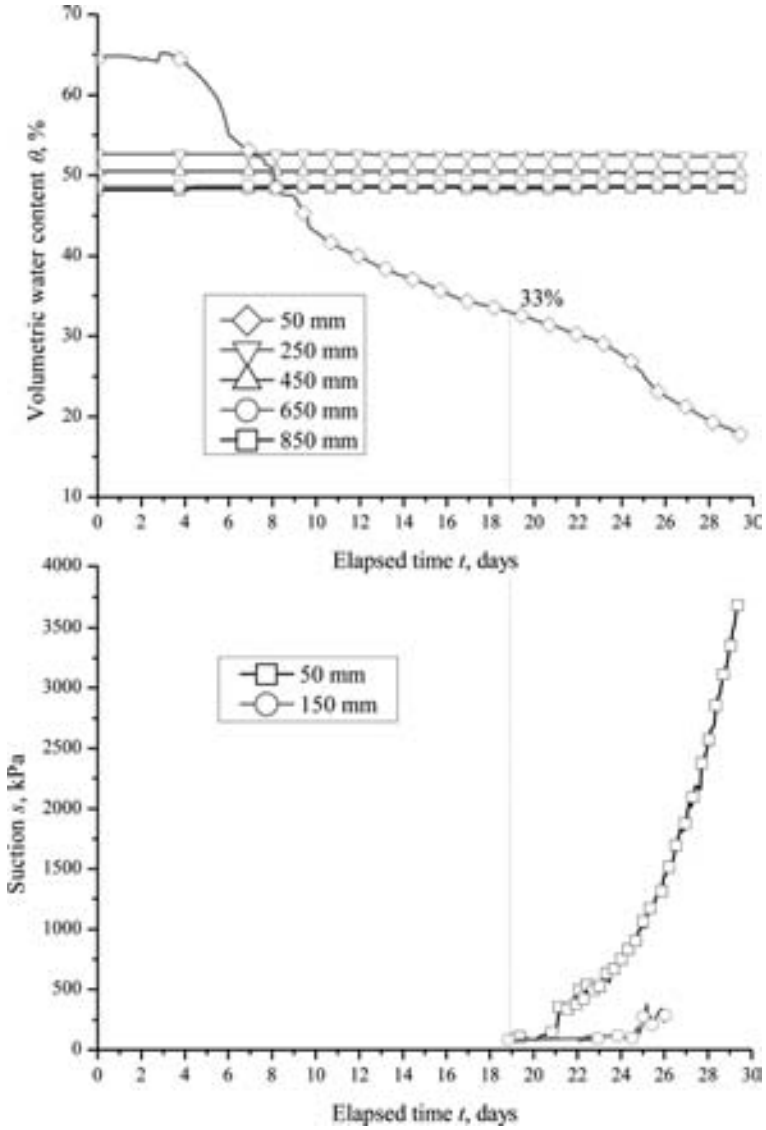

a)

b)

Fig. 5 – Variations of soil volumetric water content a) and soil suction b).
Fig. 5 – Variazione del contenuto d'acqua volumetrico a) e della suzione b).

drying, the AE begins to decrease even though the air temperature increases slightly (Fig. 3a). This decrease is progressive without sharp changes. However, a small rebound is observed from t = 20 days to t = 25 days. As the AE is calculated from the measured temperature and relative humidity, the increase of air temperature (Fig. 3a) must be the primary reason that results in this small rebound of evaporation rate.

Profile of water content and suction

Figure 5 presents the changes in soil volumetric water content θ and soil suction s over time. For the volumetric water content (Fig. 5a), it is observed that only the sensor at 50 mm depth presents a significant variation. Due to the thin water layer kept on the soil surface, the volumetric water content is almost constant during the first 3 days. After that, the value decreases gradually from 65 to 17 % at the end of drying. The sensors at deeper positions show no variations with values close to 50 %. This suggests that evaporation occurred mainly in the near surface zone.

Figure 5b presents significant variations of suction measured by two PS sensors afte about 19 days of drying (the values before are zero, showing that the soil was saturated). At 50 mm depth, a siginicant increase of suction can be noted from about 80 to 4000 kPa, and the corresponding volumetric water content decreases from about 33 to 17 % (Fig. 5 a). The significant increase of suction suggests that the soil at 50 mm depth becomes unstaturated after about 19 days. This is because, if an initially saturated soil is subjected to drying, suction will increase quickly after the air-

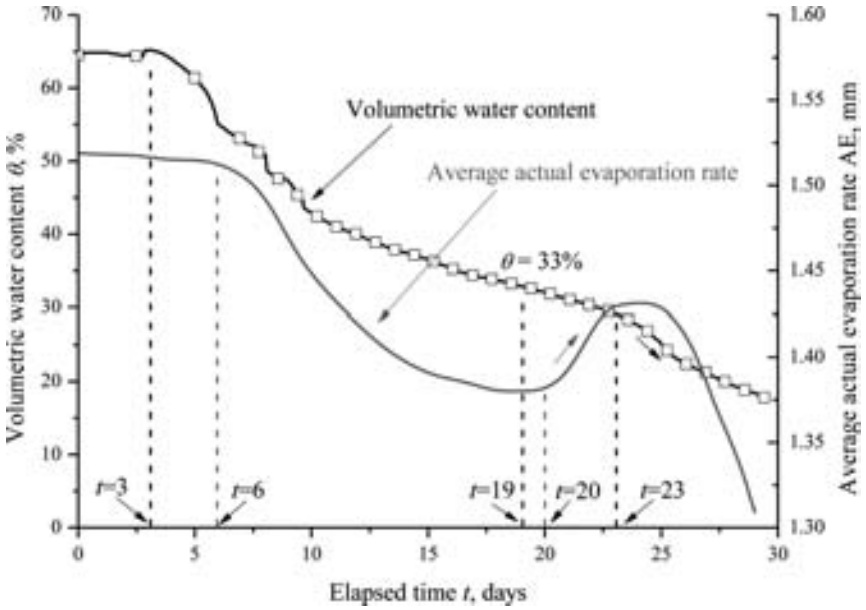

Fig. 6 – Variations of volumetric water content at 50 mm depth and average actual evaporation rate.
Fig. 6 – Variazioni del contenuto d'acqua volumetrico misurate a 50 mm di profondità durante l'essiccamento e tasso di evaporazione reale medio.

entry value is reached. The air-entry value is generally considered as a transition point where soil changes from saturated state to unsaturated state. The results also indicate that a large amount of water was lost, θ decreased from 65 % to 33 %, while soil still remained saturated before t = 19 days. This is because significant soil swell occured during the former wetting period, leading to a significant increase in void ratio and pore size for the upper soil layer. During the subsequent drying, the decrease of water content was accompanied by equivalent volumetric shrinkage until the air-entry value (θ =33%) was reached. Suction might also develop during this process, but was not measured by the PS sensor whose lower limit is estimated at 50 kPa. At 150 mm depth, obvious increase of suction is observed after about 24 days, 5 days later than that at 50 mm depth. At deeper level, as the suction is lower than the lower limit of PS sensor (50 kPa), no results are available. Based on the measured volumetric water content and suction, it can be deduced that the depth affected by this drying process is less than 250 mm.

Combining the measured volumetric water content at 50 mm depth and the average actual evaporation rate results in one plot, as shown in figure 6, more useful information can be identified. For instance, the AE curve shows that the soil in the near surface zone becomes unsaturated at t = 6 days (AE changes from constant rate to falling rate). While for the soil at 50 mm depth, it becomes unsaturated at t = 19 days, which is 13 days later than the upper soil surface. This can be attributed to the effect of transient water flow in profile. In addition, an increase of actual evaporation rate is observed at t = 20 days. A quicker decrease of volumetric water content is then observed at 50 mm depth three days later (t = 23 days). This phenomenon confirms again the effect of transient water flow in profile.

Although the soil at 50 mm depth starts to lose water from t = 3 days, it becomes unsaturated only after t = 19 days, as mentioned above. During this period, the volumetric water content decreases by 32 %, and equivalent volumetric shrinkage occurred simultaneously. TANG *et al.* [2009] indicated that the final measured saturated volumetric water content at 50 mm is about 77% after the first long wetting. The value after the second wetting becomes 65%, lower than that after the first wetting (77%) but remaining much higher than 33% measured during drying (Fig. 6). It indicates that the final measured saturated volumetric water content of soil significantly depends on wetting/drying paths. This can be attributed to the irreversible volume changes during wetting (swelling) and drying (shrinkage).

Based on the measured volumetric water content and suction at 50 mm depth during drying (Fig. 5), the water retention curve of the soil can be determined. The best fit curve obtained from the model of van GENUCHTEN [1980] is shown in figure 7. The model equation is expressed as:

$$\theta = \theta_r + \frac{\theta_s - \theta_r}{[1+(\alpha S)^n]^m} \qquad (5)$$

where θ is the volumetric water content; θr is the residual volumetric water content (6%); θs is the volumetric water content in saturated state (33%); s is suction; a, n and m are constants, equal to 0.001 kPa-1, 1.35 and 0.41, respectively.

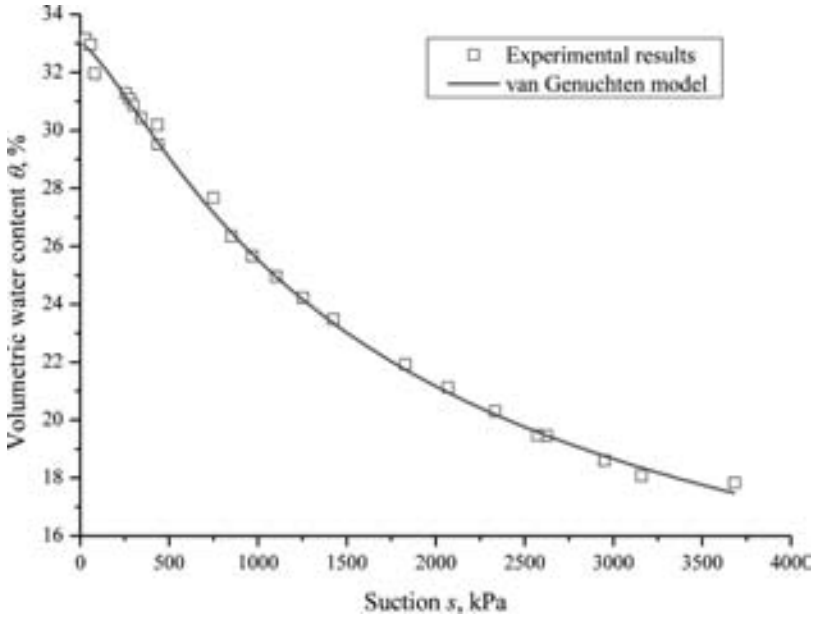

Fig. 7 – Suction and volumetric water content measured at 50 mm depth during drying.
Fig. 7 – Suzione e contenuto d'acqua volumetrico misurati a 50 mm di profondità durante l'essiccamento.

Desiccation cracking

After about 4 days of drying, cracks started to initiate on soil surface. This initiation corresponds almost to the beginning of the decrease of evaporation rate (Fig. 4). A time series of images is presented in figure 8 to describe the evolution characteristics of crack pattern. It is noted that the trace of the crack network developed in the former drying cycle can still be identified clearly even though the cracks are closed during the subsequent long period wetting (Figs. 8a-b). As the soil column is dried again, cracks generally appear at the same locations as the former drying cycle (Figs. 8b-c). This phenomenon is consistent with the results of YESILLER *at al.* [2000] and TANG *et al.* [2007], and can be explained by the destruction of some particle bonds during the former drying cycle, facilitating the initiation of cracks. Generally, the bonds are due to the various inter-particle physicochemical forces such as (1) van der Waals attraction, (2) electrical double repulsion or attraction, (3) cementation by solute precipitation, and (4) capillary attraction due to the existence of water bridges or bodies between particles. Upon wetting, the broken bonds may attract water and become weak zones in the soil. The subsequent drying causes shrinkage and cracks occur in these weak zones.

Upon further drying, cracks tend to intersect with each other and form a connected polygon network. The soil surface is split into several clods (Fig. 8 (c-f)). The intersection points of cracks form "T" and "Y" shapes. Some cracks which initiated later stop propagating, leaving a dead-end crack without intersecting. These secondary cracks are much slender than the primary cracks initiated at the same locations during the former drying. Moreover, it is interesting to note that the cracks at the boundaries are mostly perpendicular to the boundary direction. This phenomenon can be attributed to the "boundary effect" of desiccation cracking. During drying, the shrinkage of soil column results in de-bonding of soil from the vertical walls of the chamber and creates cracks along the boundary direction. Then the strain energy is released and the maximum tensile stress direction induced by shrinkage tends to be parallel to the boundary direction. It is well known that the desiccation crack results from tensile failure and always tends to grow in the direction perpendicular to the maximum tensile stress. Actually, this phenomenon and the involved mechanisms are consistent with the observation of TANG *et al.* [2011c], indicating that the initial growth direction of new cracks is generally perpendicular to the existing cracks.

For better understanding the crack evolution behaviour, the crack patterns are quantified by image processing and the geometrical and morphyologic parameters of the crack networks are determined. For simplicity and clarity, it is assumed that the water content in 0-50 mm depth is uniform during drying. With the reference of measured volumetric water content at 50 mm depth (Figs. 6 and 7), the evolution characteristics of crack parameters with water content is plotted in figure 9.

Figure 9a presents the variation of surface crack ratio R_{sc} with volumetric water content. The related suction (at 50 mm depth) is also shown in this figure for reference. Note that the suction values are determined based on the relationship illustrated in figure 7. It can be seen that cracks initiate at about 60 % water content, where the soil is still saturated. This

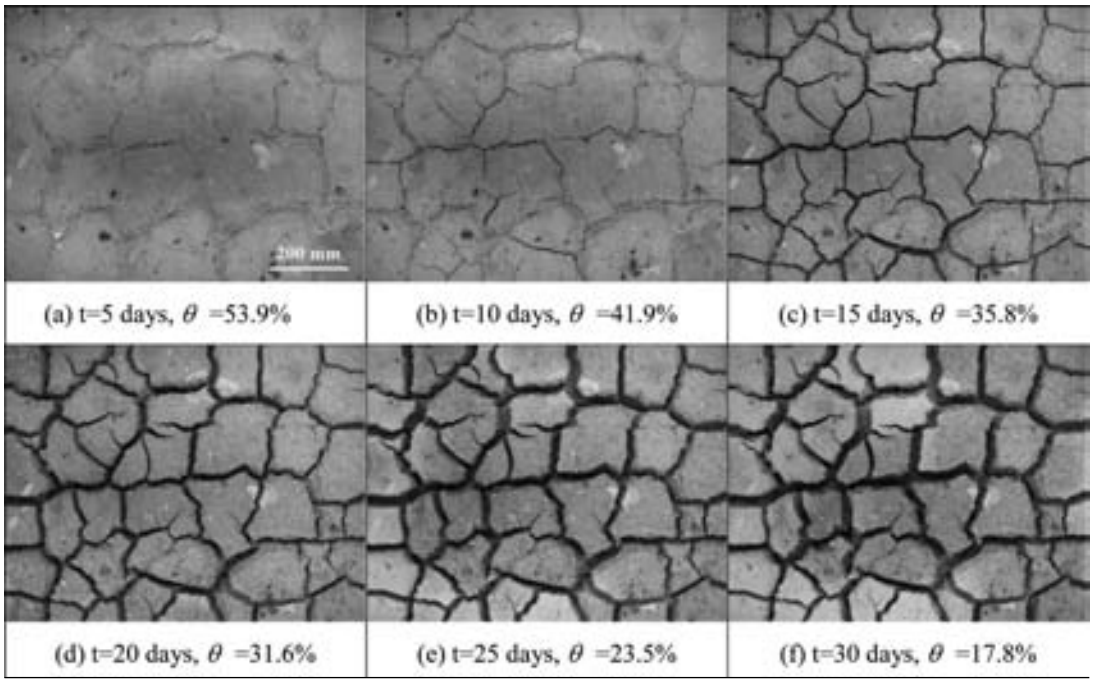

Fig. 8 – Evolution of crack patterns during drying.
Fig. 8 – Evoluzione dello stato di fratturazione durante l'essiccamento.

agrees with the observations reported in the literature [PÉRON *et al.,* 2006; RODRÍGUEZ *et al.,* 2007; TANG *et al.,* 2010; TANG 2011b]. With decreasing water content, the R_{sc} increases gradually and the final value is 33.7 %. It indicates that 33.7 % of the soil surface is covered by cracks (Fig. 8f). According to TANG *et al.* [2011c] who performed desiccation tests on the same soil, the R_{sc} reaches stabilization once the shrinkage limit (about 11%) of the soil is reached. The obtained R_{sc} in the present study does not correspond to the stage of stabilization, and it would increase upon further drying. However, the current value of R_{sc} is still much higher than the final value (about 14%) obtained by TANG *et al.* [2011c]. This may be related to the different test methods employed in the two studies. In the study of TANG *et al.* [2011c], thin (8 mm in depth) slurry specimens with small size (117 mm in diameter) were tested. Apparently, using a small-size specimen decreases the extent of soil cracking.

Figure 9b shows the variations of number of clods N_c and average area of clods A_{av} during drying. At the initial stage of cracking, several cracks appear in some locations but do not connect to each other to form separate clods. The whole soil surface is considered as an only big clod. As the water content is lower than 41.9 %, the N_c increases quickly from 1 to 7, resulting in significant decrease of A_{av}. This phenomenon is confirmed by the crack patterns shown in figures 8 a and b. Afterwards, the N_c increases progressively and finally reaches stabilization at θ = 32.5 %. It means that no new clods are split upon drying. The final stabilized value of N_c is 41. Although the N_c keeps constant during the subsequent drying period, the corresponding A_{av} still decreases gradually, as the inset plot shown in figure 9 b. This suggests that cracks keep growing during the whole drying period.

As far as the number of nodes N_n and number of crack segments N_{seg} are concerned (Fig. 9 c), it is observed that parameters N_n and N_{seg} show similar pattern during drying. They increase quickly after the water content is lower than 47.6 % and also reach stabilization as the water content reaches 32.5 %, suggesting that no new cracks initiate upon further drying, in agreement with the crack patterns presented in figures 8(d-e). TANG *et al.* [2008] reported that the final ratio of the number of crack segments to the number of intersections falls in the range of 1.5-2.0. In this investigation, the final ratio of N_{seg}/N_n is 1.38, slightly lower that the values of TANG *et al.* [2008]. This is mainly because some dead-end cracks without intersection were included in the quantification.

For the average crack length L_{av}, it generally decreases with decreasing water content and reaches stabilization at the same water content (θ = 30.7 %) as N_c. The final L_{av} is 84.2 mm. The variation of average crack width W_{av} with decreasing water content is similar to that of R_{sc} (Fig. 9a). It increases slowly at the initial stage of cracking and quickly when the water content is lower than 41.9% (Fig. 8b). At the end of drying, the final value of W_{av} is 19.1 mm.

Basically, the crack density D_c shown in figure 9e is controlled by both N_{seg} and L_{av}. The result indi-

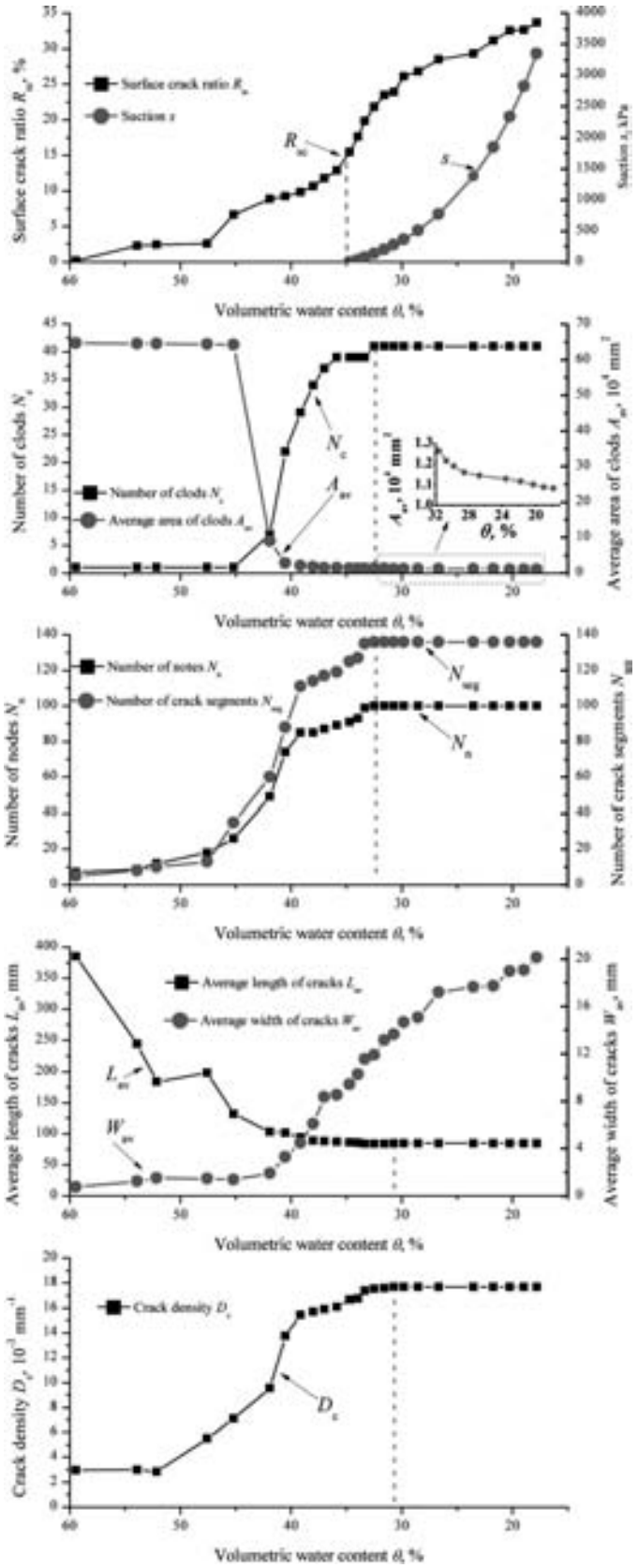

Fig. 9 – Variations of crack parameters with water content during drying : a) surface crack ratio R_{sc} and suction s; b) number of clods N_c and average area of clods A_{av}; c) number of nodes N_n and number of crack segments N_{seg}; d) average crack length L_{av} and width W_{av}; e) crack density D_c.

Fig. 9 – Variazione delle caratteristiche geometriche delle fratture in funzione del contenuto d'acqua: a) rapporto tra area delle fratture e della superficie del modello R_{sc} e suzione s; b) numero di zolle N_c e loro area media A_{av}; c) numero di nodi N_n e numero di segmenti di frattura N_{seg}; d) lunghezza media delle fratture L_{av}; e) densità delle fratture.

cates that the variation of D_c with water content is apparently dominated by N_{seg} because both the D_c and N_{seg} present similar changes. Note however that parameter D_c reaches stabilization at the same water content (θ = 30.7 %) as L_{av}.

Based on the crack parameters shown in figure 9, it is observed that N_c, N_n, N_{seg}, L_{av} and D_c can reach stabilization before the end of drying. N_c, N_n and N_{seg} reach stabilization first at a volumetric water content of 32.5 %. This suggests that the outline of the crack pattern will not change significantly because no new cracks will initiate and no crack intersections will occur during the subsequent drying. But the L_{av} and D_c still increases until a volumetric water content of 30.7 % is reached. This is due to the propagation of some pre-existent dead end cracks segments. As far as the R_{sc} is concerned, it is only contributed by the widening of crack width, as shown in figures 8 (d-e).

Conclusions

A 30-day drying test was carried out in a specially developed large scale environmental chamber to investigate the desiccation cracking behaviour of soil. The crack initiation and propagation were monitored and the crack patterns were quantitatively analysed by image processing. The following conclusions can be drawn:

1) The developed chamber allows full monitoring of air parameters (temperature, relative humidity) and soil parameters (profile water content, suction and surface cracking) as well as the determination of soil evaporation rate. The results show that the chamber constitutes an effective tool for studying the desiccation cracking behaviour of soil at large scale.
2) The data of both volumetric water content and suction show that evaporation occurred mainly in the near surface zone. The affected depth of evaporation is limited to 250 mm. The average actual evaporation rate was nearly constant as the soil was saturated and started to decline once the soil became unsaturated.
3) At onset of cracking, the soil was still saturated and the actual evaporation rate was still constant. The cracks mainly initiated at the same locations as during the former drying cycle. With further drying, the cracks are connected to each other to form a polygon network with typical "T" and "Y" shape intersections.
4) During drying, all the crack parameters reached stabilization but with different sequences. The results of this test show that the parameters N_c, N_n and N_{seg} reached stabilization first, followed by L_{av} and D_c. The parameters R_{sc} and W_{av} reached stabilization last.

Acknowledgements

This work was supported by the National Natural Science Foundation of China (Grant No. 41072211, 41322019) and Natural Science Foundation of Jiangsu Province (Grant No. BK2011339). The authors want address their thanks to Mr. De-Yin Wang of Nanjing University for his contribution to the quantification of the crack patterns.

References

ALBRECHT B.A., BENSON C.H. (2001) – *Effect of desiccation on compacted natural clay.* Journal of Geotechnical and Geoenvironmental Engineering, 127, n. 1, pp. 67-75.

ASKARINEJAD A., CASINI F., BISCHOF P., BECK A., SPRINGMAN S.M. (2012) – *Rainfall induced instabilities: a field experiment on a silty sand slope in northern Switzerland*, Rivista Italiana di Geotecnica, n. 3, pp. 50-71.

AUDIGUIER M., GEREMEW Z., LARIBI S., COJEAN R. (2007) – *Laboratory characterization of clayed soils to shrinkage-swelling susceptibility.* Revue française de géotechnique, 120–121, nn. 3-4, pp. 67-82.

BAKER R. (1981) – *Tensile strength, tension cracks, and stability of slopes.* Soils and Foundations, 21, n. 2, pp. 1-17.

CORTE A., HIGASHI A. (1960) – *Experimental research on desiccation cracks in soil.* Research report 66, U.S. Army Snow Ice and Permafrost Research Estabilishment, Wilmette, Illinois.

CUI Y.J., MANTHO A.T., CUI K., AUDIGUIER M. (2006) – *Water retention properties and volume change behaviour of natural Romainville clay.* In: Miller G.A., Zapata C.E., Houston S.L., Fredlund D.G. (Eds.), "Fourth International Conference on Unsaturated Soils" (UNSAT'2006), 873-882. American Society of Civil Engineers, Reston, VA 20191–4400, USA.

CUI Y.J., TA A.N., HEMMATI S., TANG A.M., GATMIRI B. (2013) – *Experimental and numerical investigation of soil-atmosphere interaction.* Engineering Geology, 165, pp. 20-28.

HARIANTO T., HAYASHI S., DU Y.J., SUETSUGU D. (2008) – *Effects of fiber additives on the desiccation crack behavior of the compacted Akaboku soil as a material for landfill cover barrier.* Water Air Soil Pollut., 194, nn. 1-4, pp. 141-149.

LAKSHMIKANTHA M.R, PRAT P.C., LEDESMA A. (2009) – *Image analysis for the quantification of a developing crack network on a drying Soil.* Geotechnical Testing Journal, 32, n. 6, pp. 505-515.

LAKSHMIKANTHA M.R., PRAT P.C., LEDESMA A. (2012) – *Experimental evidence of size effect in soil cracking.* Canadian Geotechnical Journal, 49, n. 3, pp. 264-284.

LARIBI S., AUDIGUIER M., COJEAN R. (2008) – *Assessing shrink/swell properties of two argillaceous soils from the Paris Basin: A comparison of cation exchange determination methods.* Bulletin of Engineering Geology and the

Environment, 67, n. 3, pp. 415-424.
MILLER C.J., MI H., YESILLER N. (1998) – *Experimental analysis of desiccation crack propagation in clay liners.* Journal of the American Water Resources Association, AWRA, 34, n. 3, pp. 677-686.
MILLER C.J., RIFAI S. (2004) – *Fiber reinforcement for waste containment soil liners.* Journal of Environmental Engineering, ASCE, 8, pp. 891-895.
MOHAMED A.A., SASAKI T., WATANABE K. (2000) – *Solute transport through unsaturated soil due to evaporation.* Journal of Environmental Engineering, 126, n. 9, pp. 842-848.
MORRIS P.H., GRAHAM J., WILLIAMS D.J. (1992) – *Cracking in drying soils.* Canadian Geotechnical Journal, 29, pp. 263-277.
NAHLAWI H., KODIKARA J.K. (2006) – *Laboratory experiments on desiccation cracking of thin soil layers.* Geotechnical and Geological Engineering, 24, pp. 1641-1664.
PÉRON H., HERCHEL T., LALOUI L., HU L.B. (2009) – *Fundamentals of desiccation cracking of fine-grained soils: experimental characterization and mechanisms identification.* Canadian Geotechnical Journal, 46, pp. 1177-1201.
PIRONE M., DAMIANO E., PICARELLI L., OLIVARES L., URCIUOLI G. (2012) – *Groundwater-atmosphere interaction in unsaturated pyroclastic slopes at two sites in Italy.* Rivista Italiana di Geotecnica, n. 3, pp. 29-49.
RIDLEY A.M. (2012) – *Relationships between climate, vegetation, pore water pressures and the serviceability of clay slopes.* Rivista Italiana di Geotecnica, n. 3, pp. 15-28.
RODRÍGUEZ R., SÁNCHEZ M., LEDESMA A., LLORET A. (2007) – *Experimental and numerical analysis of desiccation of a mining waste.* Canadian Geotechnical Journal, n. 44, pp. 644-658.
SHERARD J.L. (1973) – *Embankment dam cracking.* Embankment-dam engineering, Volume Casagrande, Wiley, New York, pp. 271–353.
SILVESTRI V., SARKIS G., BEKKOUCHE N., SOULIÉ M. (1992) – *Evapotranspiration, trees and damage to foundations in sensitive clays.* Proc., Canadian Geotechnical Conf., vol. II, pp. 533-538
TANG C.S., CUI Y.J., TANG A.M., SHI B. (2010) – *Experiment evidence on the temperature dependence of desiccation cracking behavior of clayey soils.* Engineering Geology, 114, p. 261-266.
TANG C.S., CUI Y.J., SHI B., TANG A.M., LIU C. (2011b) – *Desiccation and cracking behaviour of clay layer from slurry state under wetting-drying cycles.* Geoderma, 166, n. 1, pp. 111-118.
TANG C.S., SHI B., CUI Y.J., LIU C., GU K. (2012) – *Desiccation cracking behavior of polypropylene fiber reinforced clayey soil.* Canadian Geotechnical Journal, 49, n. 9, pp. 1088-1101.
TANG C.S., SHI B., LIU C., ZHAO L., WANG B. (2008) – *Influencing factors of geometrical structure of surface shrinkage cracks in clayey soils.* Engineering Geology, 101, pp. 204-217.
TANG C.S., SHI B., LIU C., GAO L., INYANG H.I. (2011a) – *Experimental investigationof the desiccation cracking behavior of soil layers during drying.* Journal of Materials in Civil Engineering, 23, n. 6, pp. 873-878.
TANG C.S., SHI B., LIU C., SUO W.B., GAO L. (2011c) – *Experimental characterization of shrinkage and desiccation cracking in thin clay layer.* Applied Clay Science, 52, pp. 69-77.
TANG A.M., TA A.N., CUI Y.J., THIRIAT J. (2009) – *Development of a large-scale infiltration tank for determination of the hydraulic properties of expansive clays.* Geotechnical Testing Journal, 32, n. 5, pp. 385-396.
WILSON G.W., FREDLUND D.G., BARBOUR S.L.(1997) – *The effect of soil suction on evaporative fluxes from soil surface.* Canadian Geotechnical Journal, 34, pp. 145-155.
YESILLER N., MILLER C.J., INCI G., YALDO K. (2000) – *Desiccation and cracking behavior of three compacted landfill liner soils.* Engineering Geology, 57, p. 105-121.

Indagine sperimentale sulla fratturazione da disseccamento del terreno per mezzo di camera ambientale

Sommario

La fratturazione del terreno per disidratazione è un fenomeno naturale comune e può influenzare le prestazioni del terreno in varie applicazioni nei campi della geotecnica, della geologia e dell'ingegneria ambientale. In questo studio è stata sviluppata una grande camera ambientale (1 m × 0.8 m × 1.5 m) per realizzare prove di essiccamento su modello fisico. La camera è stata strumentata con diversi sensori per il monitoraggio a varie profondità del contenuto d'acqua volumetrico e della suzione. È possibile anche la misura della temperatura e dell'umidità relativa dell'aria in ingresso, nella camera e in uscita. Lo sviluppo delle fratture sulla superficie del terreno è stato monitorato attraverso una telecamera montata al di sopra della camera. La colonna di terreno è stata sottoposta per trenta giorni ad essiccamento controllando le condizioni dell'aria. I risultati indicano che l'evaporazione reale media della colonna di terreno è costante all'inizio del processo di condizionamento e successivamente tende a decrescere col diminuire del contenuto d'acqua. Le fratture iniziano a formarsi ad elevati valori del contenuto d'acqua (circa 60%) quando il terreno è ancora saturo e il corrispondente tasso di evaporazione è costante. L'evoluzione dei parametri geometrici e morfologici del reticolo di fratture è stata analizzata con tecniche di elaborazione di immagine. Si è riscontrato che le caratteristiche delle fratture così misurate si stabilizzano a diversi valori del contenuto d'acqua durante l'essiccamento. Il numero di zolle, di nodi del reticolo e di segmenti di frattura si stabilizza prima della lunghezza media e densità delle fratture. Le caratteristiche di evoluzione del rapporto tra area delle frattura e della superficie del modello e della larghezza media delle fratture sono molto congruenti e le ultime a stabilizzarsi. I risultati indicano che la camera ambientale sviluppata rappresenta uno strumento efficace per lo studio della fratturazione da essiccamento dei terreni a grande scala e fornisce dati utili per lo studio dell'interazione terreno-atmosfera.